Nanometer-Resolved Radio-Frequency Absorption and Heating in Bio-Membrane Hydration Layers

Stephan Gekle*,† and Roland R. Netz‡

†*Fachbereich Physik, Universität Bayreuth, Germany*

‡*Fachbereich Physik, Freie Universität Berlin, Germany*

E-mail: stephan.gekle@uni-bayreuth.de

Keywords: electromagnetic absorption spectrum, lipid bilayer, molecular dynamics, dielectric heating, specific absorption rate (SAR), mobile phone [1]

Abstract

Radio-frequency (RF) electromagnetic fields are readily absorbed in biological matter and lead to dielectric heating. To understand how RF radiation interacts with macromolecular structures and possibly influences biological function, a quantitative description of dielectric absorption and heating at nanometer resolution beyond the usual effective medium approach is crucial. We report an exemplary multi-scale theoretical study for bio-membranes that combines i) atomistic simulations for the spatially resolved absorption spectrum at a single planar DPPC lipid bilayer immersed in water, ii) calculation of the electric field distribution in planar and spherical cell models, and iii) prediction of the nanometer resolved temperature profiles under steady RF radiation. Our atomistic simulations show that the only 2 nanometer thick lipid hydration layer strongly absorbs in a wide RF range between 10MHz and 100 GHz. The

[1] **Published as**: J. Phys. Chem. B **118**, 4963-4969 (2014), 10.1021/jp501562p

absorption strength, however, strongly depends on the direction of the incident wave. This requires modeling of the electric field distribution using tensorial dielectric spectral functions. For a spherical cell model, we find a strongly enhanced RF absorption on an equatorial ring, which gives rise to temperature gradients inside a single cell under radiation. Although absolute temperature elevation is small under conditions of typical telecommunication usage, our study points to hitherto neglected temperature gradient effects and allows to predict thermal RF effects on an atomistically resolved level. In addition to a refined physiological risk assessment of RF fields, technological applications for controlling temperature profiles in nano devices are possible.

Introduction

The steady increase in wireless telecommunication over the last years urgently poses the question about physiological side effects when biological tissue is exposed to electromagnetic (EM) radiation.[1,2] Although recent NMR techniques have the potential to significantly improve spatial resolution,[3] current experimental techniques[4,5] are limited to measuring the absorption and temperature rise in macroscopic pieces of biological materials with extensions much larger than a single cell. Likewise, theoretical and computational models usually assume effective, spatially homogeneous dielectric material properties.[4,6–8] This is particularly worrisome since cognitive function and signaling primarily happens at membrane surfaces.[9] Consequently any slight local temperature perturbation close to membranes, which would not be accounted for in models or measurements targeting only macroscopic heat effects, could have subtle effects on, e.g., higher brain function or immunological response. Such local effects could possibly be related to the significant effects RF radiation has on crucial cell function such as gene expression[10] or apoptosis.[11] In fact, recent spectroscopic experiments demonstrated that the biologically relevant hydration water[12–15] interacts with radiation differently from bulk water,[16–18] but the absorption of biological interfaces in the relevant RF spectral range and the spatial scale over which such interfaces absorb radiation is not known

in detail.

In this work, we show how computer simulations combined with continuum modeling can quantitatively predict temperature profiles at biological interfaces on the nanometer scale. We first present extensive Molecular Dynamics computer simulations that yield spatially resolved RF absorption spectra at a single dipalmitoylphosphatidylcholine (DPPC) lipid bilayer, which is the main constituent of typical cell membranes. The RF absorption exhibits pronounced anisotropy: for electric fields perpendicular to the membrane the absorption in the interfacial region is strongly reduced compared to bulk water, while the interfacial absorption spectrum for parallel fields shows an additional absorption peak around 30MHz in agreement with experimental bulk data.[19,20] Based on these simulation data we use continuum electrodynamic theory to predict the electric field distributions and the local specific absorption rate distributions (SAR) for simplified planar and spherical model cells. Previous modeling attempts have been severely hindered by the difficulty to obtain appropriate spatially resolved, anisotropic absorption spectra and have therefore mostly been restricted to isotropic model systems.[21–23] For the spherical cell model we find strongly enhanced local absorption on an equatorial circle for small and intermediate cell radii. In the third step we use a continuum heat conduction model and predict the steady-state temperature profile for single cells as well as for a stack of planar cells that mimics the typical arrangement of keratinocyte skin cells. We find that for RF field strengths commonly encountered in telecommunication usage, the excellent heat conductivity of the interfacial region compensates the enhanced interfacial RF absorption, such that the resulting temperature elevation does not exceed a few microkelvin. Since in the RF frequency range ionic conductivity and magnetic power dissipation is negligible and therefore dielectric heating constitutes the main biological effect,[24] we conclude that RF radiation effects are far below physiologically relevant levels even when absorption and heating effects are resolved on the nanometer level. Conversely, our methods allow to clearly predict at which radiation dosage local temperature thresholds are reached. Although our MD simulations are done for lipid bilayers, we expect the

interfacial layers around other polar biological surfaces formed by proteins or nucleic acids not to differ in major aspects and therefore our findings to apply also to cell organelles and macromolecular assemblies. Finally, the local heating effects predicted by us can be used to achieve steady state temperature gradients in closed microfluidic compartments, which opens attractive experimental routes for the study of non-equilibrium biophysical processes.[25]

Methods

Simulations

Simulations are run using the GROMACS package[26] at a temperature of 320K in order to keep the membrane in the fluid state representative of the in vivo situation,[27] for more details see the SI.

Spatially resolved tensorial absorption spectra

The spatially resolved dielectric tensor on the linear response level follows from thermal fluctuations of the local polarization vector $\mathbf{P}(z)$. In anisotropic systems such as the present one, the dielectric boundary conditions need to be properly considered.[28] Defining the polarization correlation function

$$c_\alpha(z,t) = \langle \mathbf{P}_\alpha(z,0) \cdot \mathbf{M}_\alpha(t) \rangle - \langle \mathbf{P}_\alpha(z) \rangle \cdot \langle \mathbf{M}_\alpha \rangle \tag{1}$$

where $\alpha = \parallel, \perp$, $\mathbf{M}(t) = \int_V P(t) dV$ denotes the overall system dipole moment and $\langle \ldots \rangle$ stands for time averages, the parallel component of the dielectric tensor in terms of the frequency f is

$$\epsilon_\parallel(z,f) = 1 + \frac{\beta}{2\epsilon_0} \mathcal{L}[-\dot{c}_\parallel(z,t)]. \tag{2}$$

Here the dot denotes a time derivative, $\beta = \frac{1}{k_B T}$ is the inverse thermal energy, and $\mathcal{L}[g] = \int_0^\infty \mathrm{d}t e^{-i2\pi f t} g(t)$ denotes the Laplace transformation of a function $g(t)$. For the perpendicular

component we find

$$\epsilon_\perp(z,f) = \frac{\frac{\beta}{\epsilon_0}\mathcal{L}_{i2\pi f}[-\dot{c}_\perp(z,t)]}{1+\frac{\beta}{V\epsilon_0}\mathcal{L}_{i2\pi f}[-\dot{C}_\perp(t)]-\frac{\beta}{\epsilon_0}\mathcal{L}_{i2\pi f}[-\dot{c}_\perp(z,t)]}+1 \tag{3}$$

where V is the system volume and $C_\perp(t) = \langle \mathbf{M}_\perp(0)\cdot\mathbf{M}_\perp(t)\rangle - \langle \mathbf{M}_\perp\rangle\cdot\langle \mathbf{M}_\perp\rangle$ is the system correlation function. When we display dielectric spectra that are averaged over finite regions in space or over atomic populations, we use partial integrals or sums over the polarization correlation functions $c_\alpha(z,t)$. Similar expressions have been used in the static limit.[29] The full derivation and details on the numerics are given in the SI.

SAR for spherical cell model

The time-dependent electric potential $\phi(r,\theta,t)$ satisfies the equation

$$\nabla\cdot\underline{\epsilon}(r)\nabla\phi(r,\theta,t) = 0 \tag{4}$$

where $\underline{\epsilon}(r)$ denotes the spatially dependent tensorial dielectric function which due to symmetry depends only on r. Inside a region i, where ϵ is constant, Eq. 4 is solved using the ansatz[30,31]

$$\phi_i(r,\theta,t) = A_i e^{i\omega t} r^{\delta_i}\cos\theta + B_i e^{i\omega t}\frac{1}{r^{\delta_i+1}}\cos\theta \tag{5}$$

where $2\delta_i = -1+\sqrt{1+8\epsilon_{\parallel,i}/\epsilon_{\perp,i}}$ and A_i and B_i are complex constants whose values depend on the boundary conditions (see SI). Note that this ansatz is exact as opposed to the approximation used in.[32] Knowing the electric potential one can calculate the local electric field amplitude $\mathbf{E}^0$ and the displacement field amplitude $\mathbf{D}^0$ at each point in the cell. We note that these are, in general, not parallel due to the anisotropy in the dielectric tensor. Thus, Eq. 9 cannot be applied to calculate the absorption rate. Keeping this in mind, we

obtain an expression for the absorption rate in region i which is of the form:

$$P_i(r,\theta) = -\pi \frac{f}{\rho} \mathrm{Im}\left[\mathbf{E}^{0*} \cdot \mathbf{D}^0\right] \tag{6}$$

where * denotes the complex conjugate. The detailed calculations are given in the SI.

Temperature profiles from heat diffusion equation

Inside the bilayer core, the interfacial region and the solvent region, the steady-state temperature profile $T(\mathbf{r})$ obeys the heat diffusion equation with a source term due to dielectric heating,

$$P(\mathbf{r}) = -\frac{\lambda}{\rho} \Delta T(\mathbf{r}). \tag{7}$$

where P is the specific absorption rate (SAR) calculated above, ρ is the density and λ the thermal conductivity which we assume to be constant inside each of the three regions. Corresponding values for the perpendicular thermal conductivity in lipid bilayer systems were obtained recently as λ =0.74W/(mK) in the interfacial region and λ =0.19W/(mK) in the bilayer core region including the conductivity barrier between the two monolayers.[33] For the cytoplasm and the outer water region we use λ =0.93W/(mK) as appropriate for SPC/E water.[34] We first consider the planar cell geometry where $P(\mathbf{r}) = P_i$ is constant in each region and Eq. 7 is solved by the ansatz

$$T_i(z) = -\frac{1}{2} \frac{P_i \rho_i}{\lambda_i} z^2 + V_i z + S_i. \tag{8}$$

where V_i and S_i are constants of integration whose values are determined by imposing continuity of temperature and energy flux at the boundary between two regions (for details see the SI). At the interface between the cell and the surrounding bulk water we impose a constant temperature boundary condition and present results for the temperature difference profile $\Delta T(r)$ inside the cell. In the spherical case we assume λ=0.39W/(mK) for the lateral

heat conductivity in the bilayer core,[33] and isotropic heat conductivities in the interfacial and solvent regions. We then solve Eq. 7 numerically using a finite-difference method as detailed in the SI.

Results and discussion

Spatially resolved tensorial absorption spectra

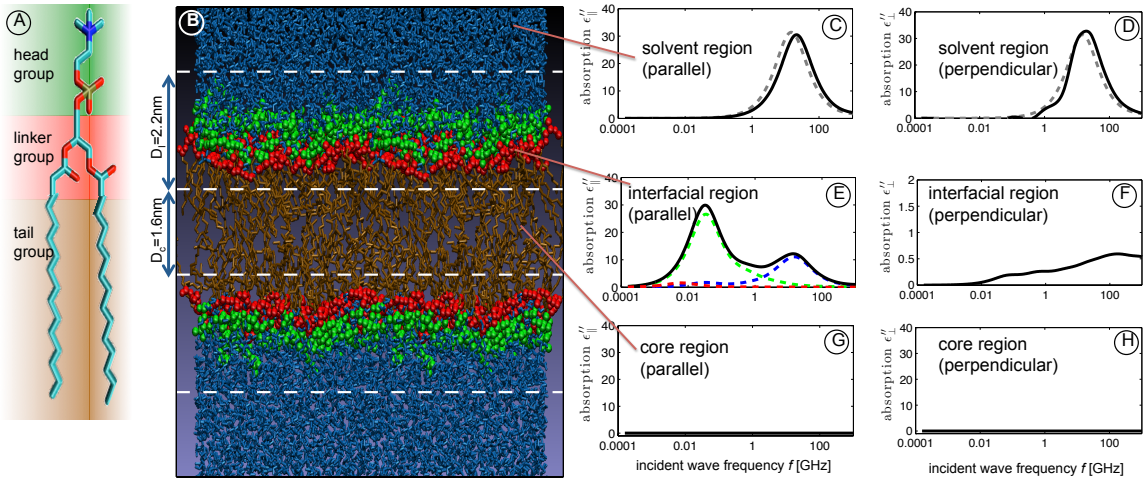

Figure 1: (A) Chemical structure of a DPPC lipid molecule. (B) Simulation snapshot: 72 DPPC molecules form a bilayer surrounded by water molecules (in blue). Lipid atoms belonging to head, linker, and tail groups are colored in green, red, and brown according to the different background color shades in A. White dashed lines separate the solvent region, the interfacial region, and the bilayer core. (C)+(D) In the solvent region, both the parallel and the perpendicular absorption spectra (solid lines) are similar to a simulated pure bulk water spectrum (dashed lines) with a dominating absorption peak at 15GHz. (E) In the interfacial region the parallel absorption spectrum $\epsilon''_{\parallel}(f)$ (black line) shows two peaks at 15 GHz and 30 MHz. The former is due to the water contribution (blue dashed line) while the latter is predominantly due to head groups (green dashed line). The linker groups (red dashed line) hardly contribute. (F) The perpendicular spectrum $\epsilon''_{\perp}(f)$ in the interfacial region is strongly attenuated (note the different scale) and the peak is shifted to significantly higher frequencies. (G)+(H) In the bilayer core there is basically no absorption.

In our Molecular Dynamics (MD) simulations we consider a periodically replicated single dipalmitoylphosphatidylcholine (DPPC) bilayer consisting of 36 lipid molecules per monolayer immersed in 2278 SPC/E water molecules, see Figure 1 A for the chemical structure

of a typical lipid molecule and Figure 1 B for a simulation snapshot. The response of a material to an electromagnetic wave is characterized by the frequency-dependent complex dielectric function $\epsilon(f) = \epsilon'(f) - i\epsilon''(f)$. Since our membrane system is anisotropic, the dielectric function is a tensor with two components $\epsilon_{\parallel}(f)$ and $\epsilon_{\perp}(f)$ for electric fields parallel and perpendicular to the membrane, respectively.[32] In order to meaningfully distinguish interfacial from bulk effects, we separately analyze the dielectric features in the bilayer core, the interfacial region and the aqueous solvent region, as indicated by broken white lines in Figure 1 B. We present results for the imaginary part of the dielectric spectrum $\epsilon''(f)$, which is proportional to the spectral absorption power; the real part, which follows from $\epsilon''(f)$ via the Kramers-Kronig relation, is presented in the Supporting Information (SI).

In the solvent region $\epsilon''(f)$ is virtually isotropic, i.e., the parallel and perpendicular components are almost indistinguishable, as shown in Figure 1 C and D. Both spectra exhibit a single prominent absorption peak at 15 GHz (solid lines) very similar to the spectrum of bulk water as obtained from simulations of 895 water molecules in the absence of the lipid layer (dashed lines). In contrast, the $D_I = 2.2$nm thick interfacial region, which entirely contains the lipid head-groups and consists of a 0.45 water and 0.55 lipid mass fraction, exhibits pronounced anisotropy. The parallel spectrum $\epsilon''_{\parallel}(f)$ in Figure 1 E displays in addition to the 15GHz water peak a prominent peak around 30 MHz. We further decompose the spectrum into contributions from hydration water, lipid head groups and lipid linker groups (see Figure 1 A for graphical definitions). The main contribution to the peak at 30 MHz comes from lipid head groups while linker groups as well as hydration water contribute only marginally in this frequency range. In fact, lipid head groups absorb also in the entire intermediate frequency range between 100 MHz and 1 GHz, in contrast to the standard interpretation of experimental bulk data where this absorption band is attributed to bound hydration water.[19] This demonstrates that water is much less dynamically "slaved" to the head group motion than commonly assumed.

The perpendicular interfacial absorption spectrum $\epsilon''_{\perp}(f)$ in Figure 1 F differs in key

aspects from the parallel one: The peak height is drastically reduced and its location is shifted by almost three orders of magnitude to around 100GHz. As we will show below, the pronounced reduction of $\epsilon''_\perp(f)$ sensitively influences the local electric field strength in non-planar membrane geometries and is thus crucial for the calculation of accurate absorption rate distributions for spherical cells. The bilayer core exhibits negligible absorption because of the absence of partial charges on the lipid tails, see Figure 1 G and H.

The pronounced absorption in the MHz range in the interfacial region is expected based on the large dipole moment of the zwitter-ionic lipid head groups. In fact, our simulated parallel spectra qualitatively match experimental absorption studies on planar membrane stacks[19] and vesicle solutions.[20] What is less expected is (i) the pronounced anisotropy with a drastically reduced perpendicular absorption strength which should be experimentally observable using surface-sensitive techniques such as time-resolved pump-probe second harmonic generation with polarized waves[35] and (ii) that the enhanced absorption in the MHz range is localized over a surprisingly thin region of only $D_I = 2.2$nm width. This immediately prompts the question whether the interfacial hydration layer can be locally heated in excess of what would be expected based on bulk studies, and whether the anisotropic dielectric structure leads to non-trivial long-ranged electrodynamic effects.

Specific absorption rates in planar and curved cell geometries

The absorption rate of electromagnetic radiation follows from the solution of Maxwell's equations which depend on the dielectric spectra. For inhomogeneous structures such as a membrane consisting of a core and interfacial regions, and in particular for curved geometries, the tensorial character of the dielectric spectra can lead to non-trivial effects. We start with the simple scenario where an EM wave vertically hits a single planar cell consisting of two parallel bilayers of infinite lateral extent that are embedded in an aqueous solvent and separated by a cytoplasmic layer, as illustrated in Figure 2 A. This geometry mimics a keratinocyte skin cell that is flattened out along the skin surface and thereby neglects

edge and curvature effects that will be treated further below. The incoming EM wave is modeled as a time-dependent and homogeneous field of the form $\mathbf{E}^{\text{ext}}(t) = \mathbf{E}_0^{\text{ext}} \cos(2\pi f t)$ that is normal to the EM propagation direction and thus parallel to the bilayer and all dielectric boundaries. For this simple geometry Maxwell's equations predict the electric field strength to be identical throughout the entire system and the perpendicular field components to vanish.[36] The specific absorption rate (SAR), which is defined as the absorbed power per unit mass, follows similarly to homogeneous, isotropic media as[37]

$$P = \pi \frac{f}{\rho} \epsilon_0 \epsilon''_{\parallel} \left| \mathbf{E}_0^{\text{ext}} \right|^2 \tag{9}$$

where ϵ_0 is the vacuum permittivity and ρ the local mass density. To obtain explicit numbers, we choose $\left|\mathbf{E}_0^{\text{ext}}\right| = 130$ V/m which corresponds to an emission source located 3cm away from the cells in vacuum with an emission power of 250mW which is typical for modern mobile phones.[38] We further select two frequencies of $f = 1.8$GHz and $f = 30$ MHz, the former is one of the frequencies used in mobile telephony while the latter represents the lower end of the very high frequency (VHF) band used, e.g., for radar applications. A frequency of 30MHz furthermore corresponds to the absorption peak in the parallel interfacial spectrum in Figure 1 E. Since the EM penetration depth for these parameters is a few centimeters and thus much larger than the cell dimensions we neglect attenuation effects of the EM wave. Using our simulation results for the dielectric absorption in the bilayer core, interfacial and solvent regions, we in Figure 2 A display the SAR distribution for 30MHz, demonstrating a highly localized maximal absorption with $P = 0.39$W/kg in the interfacial region, $P = 0$ in the core layer, and $P = 0.001$W/kg in the cytoplasm. For a frequency of f=1.8 GHz (leaving all other parameters unchanged) the corresponding SAR values are $P = 5.9$W/kg in the interfacial region, $P = 0$ in the core and $P = 6.7$W/kg in the cytoplasm (see SI). These even exceed the maximum allowed values which are $P = 1.6$W/kg in the US and between 2.0 and 4.0W/kg in Europe.[39,40] We note that for the planar scenario the SAR values are

independent of the thickness of the cytoplasm, which in Figure 2 A is taken as R_{cyto}=10nm.

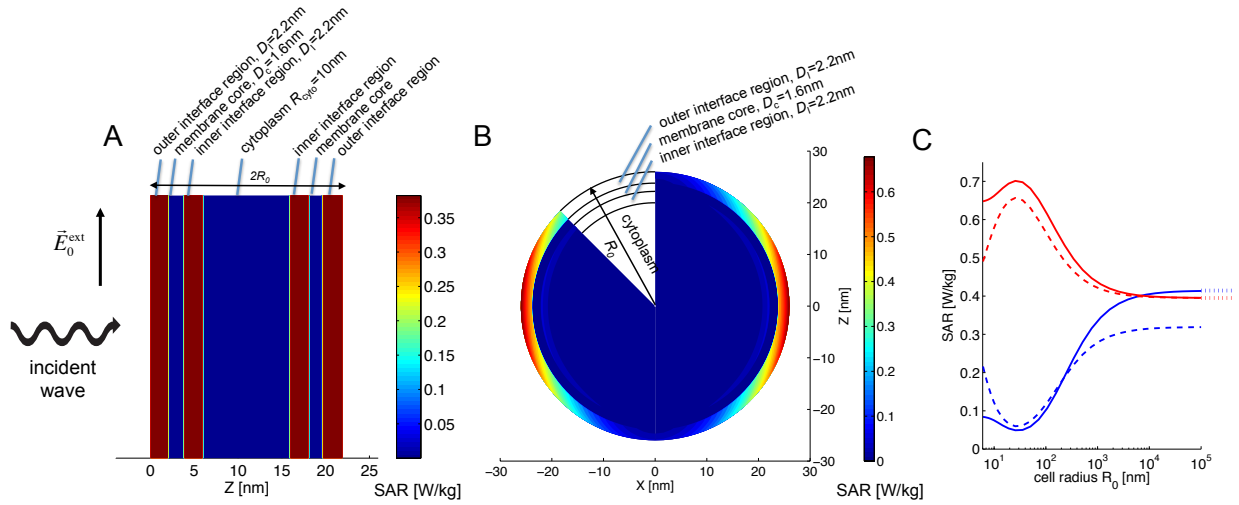

Figure 2: (A) Specific absorption rate (SAR) across a planar cell (mimicking a keratinocyte skin cell) embedded in water and normal incidence of an electromagnetic wave at 30MHz. For the interfacial and core regions with thicknesses of $D_I = 2.2$nm and $D_C = 1.6$nm, respectively, the dielectric absorption spectra from Figure 1 E and G are used. (B) For a small spherical cell/organelle with $R_0 = 26$nm outer radius under similar radiation conditions the outer interfacial equator has a SAR about 15 times larger than at the poles. In the inner interfacial region much less energy is absorbed. (C) As the cell radius R_0 increases the SARs at the outer edge of the interfacial regions at the pole (blue solid) and at the equator (red solid) approach and eventually cross. The asymptotic values are indicated by dotted lines. Comparison with a cell membrane having a fictitous isotropic dielectric absorption spectrum (dashed lines) corresponding to the parallel spectrum demonstrates the importance of the tensorial anisotropy (see main text).

We now switch to our spherical cell model, where a single bilayer encloses a spherical cytoplasm volume as illustrated in Figure 2 B. The outer radius $R_0 = R_{\mathrm{cyto}} + D_C + 2D_I$ varies between 0 and 100μm. The cell is immersed in a very large (10^5 times larger than R_{cyto}) spherical solvent reservoir. The dielectric tensor in the interfacial region is expressed in spherical coordinates with the radial and tangential components given by the perpendicular and parallel spectra $\epsilon_\perp(f)$ and $\epsilon_\parallel(f)$ taken from Figure 1 E and F, respectively. For an external electric field pointing along the z-direction the electric field distribution is inhomogeneous and anisotropic even when the dielectric membrane properties are assumed isotropic.[41] In the present case the situation is more complex due to the tensorial character of the membrane dielectric spectra, as outlined in the Methods Section. In Figure 2 B we

present the SAR distribution for an outer radius of $R_0 = 20$nm. Note that this radius is smaller than a typical cell and rather corresponds to an organelle. In fact, we use our spherical model for the whole range of outer radii from $R_0 = D_C + 2D_I = 6$nm, in which case the cytoplasmic water core is absent, to radii in the μm range. The smallest radii correspond to liposomes and presumably are not too different from proteins in their dielectric structure, since also proteins have mobile polar groups on their surface.

We first note that, in contrast to the planar cell, the SAR differs between the two lipid monolayers. The SAR values in the inner monolayer are strongly reduced due to the dielectric screening by the bilayer core. An even more striking observation is the strong angular dependence of the SAR: for the frequency 30 MHz and outer radius $R_0 = 26$nm in Figure 2 B the equator forms a focal ring with a local SAR of $P = 0.7$W/kg, even higher than obtained for the planar geometry in Figure 2 A, whereas at the poles only $P = 0.05$W/kg are absorbed. At 1.8GHz the respective values are 11.4W/kg and 2.4W/kg as shown in the SI.

In Figure 2 C we plot the SAR in the outer monolayer at the equator (red solid line) and at the poles (blue solid line) as a function of the outer cell radius. It is seen that above a few μm in radius the situation reverses and the poles become points of maximal absorption. The planar limit of infinite radius in which the pole and equatorial regions correspond to planar slabs that are oriented perpendicularly and parallel to the external field, respectively, is analytically tractable and yields $P^{\infty}_{\text{pole}} = \pi f \epsilon_0 \epsilon''_{\perp} (\left|\mathbf{E}_0^{\text{ext}}\right| |\epsilon_{\text{bulk}}| / |\epsilon_{\perp}|)^2/\rho$ and $P^{\infty}_{\text{equator}} = \pi f \epsilon_0 \epsilon''_{\parallel} \left|\mathbf{E}_0^{\text{ext}}\right|^2 /\rho$, which are indicated by blue and red dotted lines in Figure 2 C.

The importance of the interplay between the tensorial components is illustrated by calculations where the dielectric spectra in the interfacial region are fictitiously assumed isotropic. The dashed lines in Figure 2 C show the SAR at the equator and pole where both parallel and perpendicular dielectric interfacial absorption spectra are characterized by the parallel absorption spectrum of Figure 1 E. For small radii, both quantities are significantly lower than the true SAR shown by solid lines, thus demonstrating that the absorption in a spherical shell is influenced by spectral anisotropies and cannot be accounted for by a simple

geometric mixing of parallel and perpendicular components.

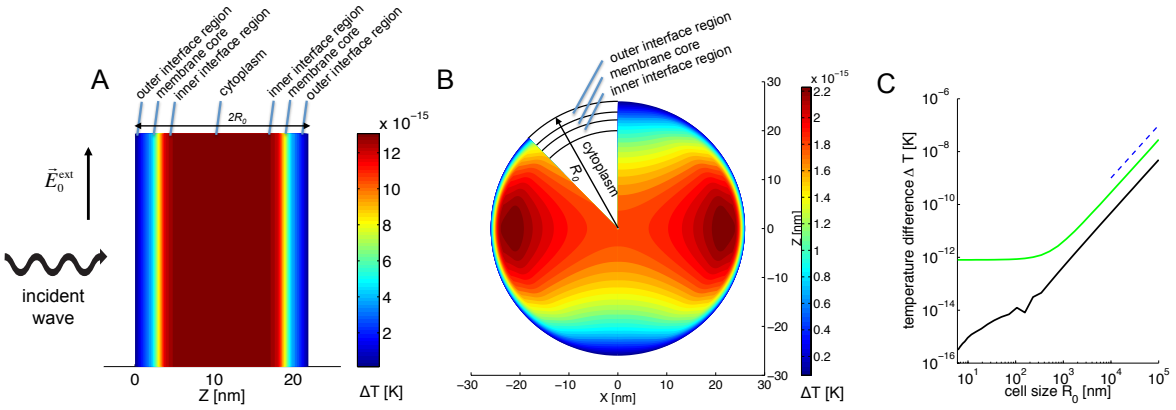

Figure 3: Excess temperature difference profiles ΔT for cells at fixed surface temperature under fixed radiation at 30 MHz with a 250mW point source at a distance 3 cm (see text) for (A) planar cell model and (B) a spherical cell model. In the spherical cell the hottest point is near the equator where the EM wave absorption is largest. (C) Maximal temperature rise as a function of cell size R_0. ΔT rises up to around 30nK for a 100μm thick planar cell (green line) and to roughly 2nK for the largest spherical cell (black line). The quadratic dependence of ΔT on R_0 for large cells (blue dashed line) is similar in both geometries and can be understood from the first term in Eq. 8. Note that the two ΔT's are not identical even for very large radii demonstrating the long-ranged influence of the curvature in the spherical case.

Temperature profiles for single cells

Using a continuum heat conduction model that incorporates the spatially dependent SAR profile from the last section we now determine the stationary temperature profile under steady irradiation (see Methods Section). As a boundary condition we fix the temperature at the outer cell surface, which can be viewed as being the result of blood perfusion. The heat conductivity parameters are taken from.[33] Figure 3 A shows the excess temperature profile ΔT compared to the fixed outer boundary value for the planar cell model with a 10nm thick cytoplasm for an EM frequency of 30 MHz. The temperature difference ΔT hardly exceeds 10^{-14}K and a physiological side effect can be clearly ruled out. Figure 3 C shows that the maximal temperature increase ΔT for the planar cell as a function of the cell size R_0 (green line) rises up to 30nK for a 100μm thick planar cell. The corresponding value for

a field frequency of 1.8GHz is around 2μK as shown in the SI.

In the spherical cell the absorbed power P exhibits a complex spatial pattern and the solution of the heat conduction equation is obtained numerically by a finite-difference method (see SI). The resulting temperature distribution in Figure 3 B locates the hottest point in the vicinity of the equator where also the absorption is largest. Increasing the cell radius only leads to a slight increase in the temperature difference up to around 2nK for a cell with a radius of $R_0 = 100\mu$m at 30 MHz as shown in Figure 3 C (black line) and up to 12μK at 1.8GHz (see SI). We see that the inhomogeneous EM power absorption is counteracted by the efficient heat conduction in the bilayer core and the interfacial region leading to relatively smooth temperature profiles.

Temperature profile in a multicellular skin model

We finally present the temperature profile when a multicellular skin patch is exposed to an EM wave incorporating the nanometer resolved absorption spectra in the cell membranes obtained by our atomistic simulations and the heat conductivity barriers in the membrane interiors. No empirical data or additional assumptions are required which is in contrast to currently used skin models.[8] We consider a stack of 110 planar keratinocyte cells as illustrated in Figure 4 A. Each cell is modeled with a 1 μm thick cytoplasmic interior. At the right end of the cell stack we impose a constant temperature mimicking blood perfusion and heat transport away from the exposed area. At the left end an insulating air layer is assumed. The resulting temperature profile is shown in Figure 4 B. At 30MHz it exhibits a maximum at the skin-air interface with a temperature about 35nK higher than that of the blood vessel. At 1.8GHz this value increases up to around 50μK.

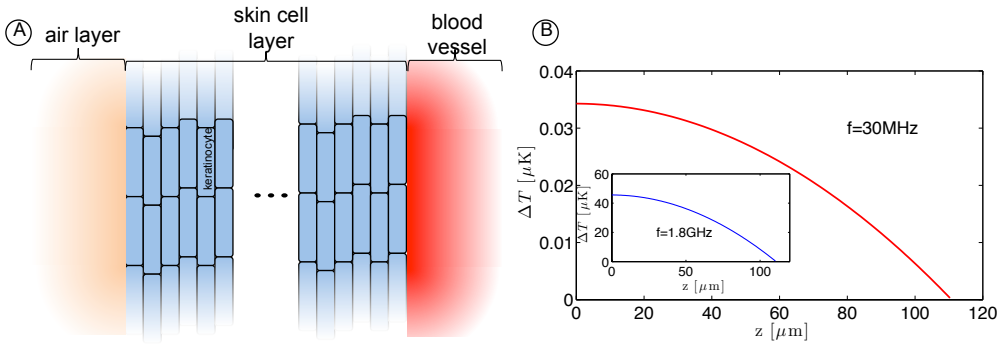

Figure 4: (A) A patch of skin is modelled as a stack of 110 planar keratinocyte cells bounded by a blood vessel on the right and a large air layer on the left. (B) The resulting temperature profile exhibits a maximum with 35nK at the air-exposed edge of the skin for a frequency f =30MHz. *Inset:* For an electromagnetic wave as typically emitted from a mobile phone with $f = 1.8$GHz the maximum temperature rise is about 50μK.

Conclusion

We have introduced a multi-scale modeling approach for the effects of dielectric heating due to RF radiation on structured biological matter for the exemplary case of a bio-membrane consisting of three consecutive steps: (i) Atomistically resolved MD simulations provide the anisotropic, frequency-dependent, spatially resolved absorption spectra of a DPPC lipid bilayer immersed in water; (ii) these tensorial spectra are then incorporated into continuum electrodynamics to calculate the electric field distributions and the resulting specific absorption rate (SAR) profiles for planar and spherical cell models; (iii) finally, the SAR profiles together with thermal conductivity data are used in conjunction with continuum heat conduction theory to predict the steady-state temperature profiles of single cells as well as tissue models composed of multiple cells.

The main finding of our atomistic simulation studies in part (i) is that the interfacial region at a lipid bilayer strongly absorbs in a wide RF range from 10 MHz to 100 GHz when the electric field is parallel to the membrane, whereas for perpendicular field orientation the absorption is much weaker than in bulk water. Such a symmetry breaking has been seen in simulations of solid surfaces before and is more a consequence of the dielectric boundary

condition than the signature of an anisotropy in the molecular mobility in the interfacial region.[32] Interestingly, the role of water for the interfacial parallel absorption is confined to the standard spectral range around 15 GHz, water is not dynamically bound or slaved to lipid molecules. Our main finding in step (ii) is that the specific absorption rate strongly varies between different points of a spherical cell: for relatively small cells (below a radius of ca. 1μm) we find strongly enhanced absorption at an equatorial ring in the outer lipid monolayer. In step (iii) we find that for fields as emitted in typical telecommunication applications the temperature elevation in an isolated cell stays below a micro-Kelvin. For a skin model composed of a stack of 110 planar keratinocyte cells the temperature rise at the air-exposed skin side is about 50μK which hardly can give rise to physiological side effects. Our results, which should also apply to organelles and other biological structures that are surrounded by polar surfaces, can be trivially scaled up by increasing the incident radiation power or by decreasing the distance to the emitter and might be useful for imposing temperature gradients in experimental micro-devices in the context of non-equilibrium thermal effects.[25]

In the future, dielectric absorption profiles should also be evaluated at other biological relevant surfaces such as proteins and nucleic acids. Dielectric anisotropy effects of the kind found by us can be straightforwardly incorporated into existing numerical schemes[4,42] and software packages for SAR prediction (SEMCAD, COMSOL, CST Microwave Studio, etc.) and should improve their accuracy thus leading to more reliable safety standards for RF exposure of biological tissue.

Acknowledgement

SG thanks the Deutsche Forschungsgemeinschaft (GE2214/1) and the Volkswagen Foundation for financial support. RRN acknowledges support from the Deutsche Forschungsgemeinschaft in the collaborative research initiative SFB 1078 "Protonation Dynamics in Pro-

tein Function". We gratefully acknowledge the Forschungszentrum Jülich and the Leibniz-Rechenzentrum for computer resources.

References

(1) *WHO Research Agenda for radiofrequency fields*; 2009.

(2) van Rongen, E.; Croft, R.; Juutilainen, J.; Lagroye, I.; Miyakoshi, J.; Saunders, R.; de Seze, R.; Tenforde, T.; Verschaeve, L.; Veyret, B.; Xu, Z. Effects of Radiofrequency Electromagnetic Fields on the Human Nervous System. *J. Toxicol. Env. Health B* **2009**, *12*, 572–597.

(3) Gultekin, D. H.; Moeller, L. NMR Imaging of Cell Phone Radiation Absorption in Brain Tissue. *Proc. Nat. Acad. Sci. (USA)* **2013**, *110*, 58–63.

(4) Gajsek, P.; Walters, T. J.; Hurt, W. D.; Ziriax, J. M.; Nelson, D. A.; Mason, P. A. Empirical Validation of SAR Values Predicted by FDTD Modeling. *Bioelectromagnetics* **2001**, *23*, 37–48.

(5) Franzellitti, S.; Valbonesi, P.; Ciancaglini, N.; Biondi, C.; Contin, A.; Bersani, F.; Fabbri, E. Transient DNA Damage Induced by High-Frequency Electromagnetic Fields (GSM 1.8GHz) in the Human Trophoblast HTR-8/SVneo Cell Line Evaluated with the Alkaline Comet Assay. *Mutat. Res. Fund. Mol. M.* **2010**, *683*, 35–42.

(6) Gabriel, S.; Lau, R. W.; Gabriel, C. The Dielectric Properties of Biological Tissues: III. Parametric Models for the Dielectric Spectrum of Tissues. *Phys. Med. Biol.* **1996**, *41*, 2271–2293.

(7) Feldman, Y.; Puzenko, A.; Ben Ishai, P.; Caduff, A.; Agranat, A. Human Skin as Arrays of Helical Antennas in the Millimeter and Submillimeter Wave Range. *Phys. Rev. Lett.* **2008**, *100*, 128102.

(8) Shafirstein, G.; Moros, E. G. Modelling Millimetre Wave Propagation and Absorption in a High Resolution Skin Model: The Effect of Sweat Glands. *Phys. Med. Biol.* **2011**, *56*, 1329–1339.

(9) van Meer, G.; Voelker, D. R.; Feigenson, G. W. Membrane Lipids: Where They Are and How They Behave. *Nature Reviews Molecular Cell Biology* **2008**, *9*, 112–124.

(10) Buttiglione, M.; Roca, L.; Montemurno, E.; Vitiello, F.; Capozzi, V.; Cibelli, G. Radiofrequency Radiation (900 MHz) Induces Egr-1 Gene Expression and Affects Cell-Cycle Control in Human Neuroblastoma Cells. *J. Cell. Physiol.* **2007**, *213*, 759–767.

(11) Joubert, V.; Bourthoumieu, S.; Leveque, P.; Yardin, C. Apoptosis is Induced by Radiofrequency Fields through the Caspase-Independent Mitochondrial Pathway in Cortical Neurons. *Radiat. Res.* **2008**, *169*, 38–45.

(12) Rasaiah, J. C.; Garde, S.; Hummer, G. Water in Nonpolar Confinement: From Nanotubes to Proteins and Beyond *. *Annu. Rev. Phys. Chem.* **2008**, *59*, 713–740.

(13) Li, J.; Fernandez, J. M.; Berne, B. J. Water's Role in the Force-Induced Unfolding of Ubiquitin. *Proc. Nat. Acad. Sci. (USA)* **2010**, *107*, 19284–19289.

(14) Baron, R.; Setny, P.; Andrew McCammon, J. Water in Cavity Ligand Recognition. *J. Am. Chem. Soc.* **2010**, *132*, 12091–12097.

(15) Thirumalai, D.; Reddy, G.; Straub, J. E. Role of Water in Protein Aggregation and Amyloid Polymorphism. *Accounts of Chemical Research* **2012**, *45*, 83–92.

(16) Pal, S. K.; Zewail, A. H. Dynamics of Water in Biological Recognition. *Chem. Rev.* **2004**, *104*, 2099–2124.

(17) Born, B.; Weingärtner, H.; Bründermann, E.; Havenith, M. Solvation Dynamics of Model Peptides Probed by Terahertz Spectroscopy. Observation of the Onset of Collective Network Motions. *J. Am. Chem. Soc.* **2009**, *131*, 3752–3755.

(18) Tielrooij, K. J.; Paparo, D.; Piatkowski, L.; Bakker, H. J.; Bonn, M. Dielectric Relaxation Dynamics of Water in Model Membranes Probed by Terahertz Spectroscopy. *Biophys J* **2009**, *97*, 2484–2492.

(19) Klösgen, B.; Reichle, C.; Kohlsmann, S.; Kramer, K. D. Dielectric Spectroscopy as a Sensor of Membrane Headgroup Mobility and Hydration. *Biophys J* **1996**, *71*, 3251–3260.

(20) Merla, C.; Liberti, M.; Apollonio, F.; d'Inzeo, G. Quantitative Assessment of Dielectric Parameters for Membrane Lipid Bi-Layers from RF Permittivity Measurements. *Bioelectromagnetics* **2009**, *30*, 286–298.

(21) Huclova, S.; Erni, D.; Fröhlich, J. Modelling Effective Dielectric Properties of Materials Containing Diverse Types of Biological Cells. *J Phys D* **2010**, *43*, 365405.

(22) Simeonova, M.; Gimsa, J. The Influence of the Molecular Structure of Lipid Membranes on the Electric Field Distribution and Energy Absorption. *Bioelectromagnetics* **2006**, *27*, 652–666.

(23) Asami, K. Dielectric Dispersion in Biological Cells of Complex Geometry Simulated by the Three-Dimensional Finite Difference Method. *J. Phys. D Appl. Phys.* **2006**, *39*, 492–499.

(24) Kotnik, T.; Miklavcic, D. Theoretical Evaluation of the Distributed Power Dissipation in Biological Cells Exposed to Electric Field. *Bioelectromagnetics* **2000**, *21*, 385–394.

(25) Mast, C. B.; Schink, S.; Gerland, U.; Braun, D. Escalation of Polymerization in a Thermal Gradient. *Proc. Nat. Acad. Sci. (USA)* **2013**, *110*, 8030–8035.

(26) Hess, B.; Kutzner, C.; van der Spoel, D.; Lindahl, E. GROMACS 4: Algorithms for Highly Efficient, Load-Balanced, and Scalable Molecular Simulation. *J. Chem. Theory Comput.* **2008**, *4*, 435–447.

(27) Schneck, E.; Sedlmeier, F.; Netz, R. R. Hydration Repulsion Between Biomembranes Results from an Interplay of Dehydration and Depolarization. *Proc. Nat. Acad. Sci. (USA)* **2012**, *109*, 14405–14409.

(28) Gekle, S.; Arnold, A. Comment on "Anomalous Dielectric Behavior of Nanoconfined Electrolytic Solutions". *Phys. Rev. Lett.* **2013**, *111*, 089801.

(29) Stern, H. A.; Feller, S. E. Calculation of the Dielectric Permittivity Profile for a Nonuniform System: Application to a Lipid Bilayer Simulation. *J. Chem. Phys.* **2003**, *118*, 3401.

(30) Roth, J.; Dignam, M. J. Scattering and Extinction Cross Sections for a Spherical Particle Coated with an Oriented Molecular Layer. *J. Opt. Soc. Am.* **1973**, *63*, 308.

(31) Sukhorukov, V. L.; Meedt, G.; Kürschner, M.; Zimmermann, U. A Single-Shell Model for Biological Cells Extended to Account for the Dielectric Anisotropy of the Plasma Membrane. *J. Electrostat.* **2001**, *50*, 191–204.

(32) Gekle, S.; Netz, R. R. Anisotropy in the Dielectric Spectrum of Hydration Water and its Relation to Water Dynamics. *J. Chem. Phys.* **2012**, *137*, 104704.

(33) Nakano, T.; Kikugawa, G.; Ohara, T. A Molecular Dynamics Study on Heat Conduction Characteristics in DPPC Lipid Bilayer. *J. Chem. Phys.* **2010**, *133*, 154705.

(34) Mao, Y.; Zhang, Y. Thermal Conductivity, Shear Viscosity and Specific heat of Rigid Water Models. *Chem Phys Lett* **2012**, *542*, 37–41.

(35) Petersen, P. B.; Saykally, R. J. Probing the Interfacial Structure of Aqueous Electrolytes with Femtosecond Second Harmonic Generation Spectroscopy. *J. Phys. Chem. B* **2006**, *110*, 14060–14073.

(36) Griffiths, D. J. *Introduction to Electrodynamics*; Prentice Hall, 1999.

(37) Böttcher, C. J. F.; Bordewijk, P. *Theory of Electric Polarization II*; Elsevier Scientific, 1978.

(38) *Exposure to high frequency electromagnetic fields, biological effects and health consequences (100 kHz - 300 GHz)*; 2009.

(39) Means, D. L.; Chan, K. W. *Evaluating Compliance with FCC Guidelines for Human Exposure to Radiofrequency Electromagnetic Fields, OET Bulletin 65 Supplement C*; 2001.

(40) COUNCIL RECOMMENDATIONof 12 July 1999on the limitation of exposure of the general public to electromagnetic fields (0 Hz to 300 GHz). *Journal of the European Communities* **1999**, *199*, 59–70.

(41) Kaatze, U. Bound Water: Evidence from and Implications for the Dielectric Properties of Aqueous Solutions. *J. Mol. Liq.* **2011**, *162*, 105–112.

(42) Zhadobov, M.; Sauleau, R.; Le Drean, Y.; Alekseev, S. I.; Ziskin, M. C. Numerical and Experimental Millimeter-Wave Dosimetry for In Vitro Experiments. *IEEE Trans. Microwave Theory Techn.* **2008**, *56*, 2998–3007.